Ain Shams Engineering Journal (2015) 6, 577–585

Ain Shams University

Ain Shams Engineering Journal

www.elsevier.com/locate/asej
www.sciencedirect.com

MECHANICAL ENGINEERING

Numerical investigation of turbulent forced-convective heat transfer of Al_2O_3–water nanofluid with variable properties in tube

Alireza Aghaei *, Ganbar Ali Sheikhzadeh, Majid Dastmalchi, Hamed Forozande

Mech. Eng., Univ. of Kashan, Kashan, Iran

Received 27 July 2014; revised 13 November 2014; accepted 23 November 2014
Available online 10 January 2015

KEYWORDS

Nanofluid;
Turbulent flow;
Forced convection;
Skin fraction;
Brownian motion;
Numerical solution

Abstract In this study, the flow field and heat transfer of Al_2O_3–water nanofluid turbulent forced convection in a tube are investigated. The surface of the tube is hot (T_h = 310 K). Simulations are carried out for constant water Prandtl number of 6.13, Reynolds numbers from 10,000, 20,000, 30,000 to 100,000, nanoparticles volume fractions of 0, 0.001, 0.1, 0.2, 0.4 and nanoparticles' diameter of 25, 33, 75, and 100 nm. The finite volume method and SIMPLE algorithm are utilized to solve the governing equations numerically. The numerical results showed that with enhancing Reynolds numbers, average Nusselt number increases. The variations of the average Nusselt number relative to volume fractions are not uniform. For all of the considered volume fractions, by increasing the Reynolds number the skin friction factor decreases and with increasing volume fractions and Reynolds number the pressure drop increases.

1. Introduction

Nanofluid is the term applied to a suspension of solid, nanometer-sized particles in conventional fluids; the most prominent features of such fluids include enhanced heat characteristics, such as convective heat transfer coefficient, in comparison with the base fluid without considerable alterations in physical and chemical properties. Nanofluids have novel properties that make them potentially useful in many applications. They show enhanced thermal conductivity compared to the base fluid. Several researches [1–3] have showed that by adding nanoparticle with low volume fraction (1–5%), the thermal conductivity can be increased by about 20%.

The first work on convective flow and heat transfer of nanofluids, was presented by Pak and Cho [4] before Choi and his group introduced the term *nano-fluids*. The first observation they made was a substantial increase in the heat transfer coefficient in the turbulent flow regime. The experiment showed the applicability of the Dittus–Boelter for pure water flow and a substantial increase in the heat transfer coefficient

* Corresponding author at: P.O.B. 87317-51167, Kashan, Iran. Tel.: +98 9135535460, +98 3155919 2446.
E-mail addresses: AlirezaAghaei21@gmail.com (A. Aghaei), sheikhz@kashanu.ac.ir (G.A. Sheikhzadeh), majid.dastmalchi@gmail.com (M. Dastmalchi), Hamed.fg.mech@gmail.com (H. Forozande).
Peer review under responsibility of Ain Shams University.

ELSEVIER Production and hosting by Elsevier

http://dx.doi.org/10.1016/j.asej.2014.11.015

for flow with the particles suspended. Also, their overall depiction is much more gloomy. They found that the Darcy friction factor follows the Kays correlation. Thus, due to a rise in viscosity, there is a substantial rise in frictional pressure-drop. This means that although the heat transfer coefficient increases in nanofluids, the pressure-drop penalty is substantial. In convection heat transfer applications there is always competition between enhancement of heat transfer and the resulting pressure penalty.

Buongiorno [5] theoretically investigated the unusual Nusselt number increase for forced convection in a duct and related this heat transfer enhancement to reduction of viscosity caused by nanoparticle transport within the boundary layer. He introduced seven transport mechanisms that cause relative velocity between nanoparticles and fluid. By comparing the diffusion timescale of transport mechanisms, he showed that the Brownian motion and thermophoresis are the two most important mechanisms.

Wesley Williams et al. [6] investigated the turbulent convective heat transfer behavior of alumina and zirconia nanoparticle dispersions in water experimentally in a flow loop with a horizontal tube test section. They find that the convective heat transfer and pressure loss behavior of nanofluids can be predicted by the traditional correlations and models, as long as the effective nanofluid properties are used in calculating the dimensionless numbers. They observe, no abnormal heat transfer enhancement. Namburu et al. [7] numerically analyzed turbulent flow and heat transfer of Al_2O_3, CuO, and SiO_2 nanoparticles suspended in ethylene glycol and water based fluids in a straight circular tube. They indicated that SiO_2 with nanoparticle diameter of 20 nm provides the highest thermal conductivity enhancement due to higher viscosity value of lower nanoparticle diameter. Fotukian and Nasr Esfahany [8,9] investigated Turbulent convective heat transfer and pressure drop of Al_2O_3/water and CuO/water nanofluid inside a circular tube experimentally. They indicated that addition of small amounts of nanoparticles to the base fluid augmented heat transfer remarkably. Increasing the volume fraction of nanoparticles in the range studied in their work did not show much effect on heat transfer enhancement. They showed that pressure drop for the dilute nanofluid was much greater than that of the base fluid. They also predicted that ejection of nanoparticles from the wall to the bulk of the flow may be responsible for considerable augmentation of heat transfer by addition of small amounts of nanoparticles to the base fluid. Demir et al. [10] investigated numerically forced convection flow of TiO_2 and Al_2O_3 nanoparticles suspended in pure water in a horizontal tube. It was found that convective heat transfer coefficient, pressure drop and wall shear stress increase with increasing Reynolds number and the higher pressure drop reported by using nanofluids due to increment on viscosity of the mixture. Bianco et al. [11] analyzed numerically the turbulent forced convection nanofluid flow with Al_2O_3 nanoparticles suspended in water passing through a circular tube. They concluded that increasing the particles concentration would increase the heat transfer coefficient. Sajadi and Kazemi [12] studied the turbulent heat transfer behavior of titanium dioxide/water nanofluid in a circular pipe under the constant wall temperature condition, experimentally. Their results showed that the heat transfer coefficient increased about 22% at a Reynolds number of 5000, for 0.25% volume fraction of TiO_2, while the pressure drop was about 25% greater than that of pure water. Zamzamian et al. [13] study the effect of forced convective heat transfer of nanofluids of aluminum oxide and copper oxide prepared in ethylene glycol in turbulent flow. They find considerable enhancement in convective heat transfer coefficient of the nanofluids as compared to the base fluid. Moreover, their results indicate that with increasing nanoparticles concentration and nanofluid temperature, the convective heat transfer coefficient of nanofluid increases. Nasiri et al. [14] investigated the turbulent heat transfer performance of Al_2O_3–H_2O and TiO_2–H_2O nanofluids through square channel with constant wall temperature boundary condition experimentally. They reported that convective heat transfer coefficient and Nusselt number of nanofluids are higher than those of distilled water. They revealed that the convective heat transfer and pressure drop of nanofluids tested in fully developed turbulent flow region can be predicted with the help of the traditional correlations and models, provided that the effective nanofluid properties are used in calculating the dimensionless numbers. Corcione et al. [15] study heat transfer of nanoparticle suspensions in single-phase turbulent pipe flow theoretically. They extended the convective heat transfer correlations available in the literature for single-phase flows to nanoparticle suspensions, provided that the thermophysical properties appearing in them are the nanofluid effective properties calculated at the reference temperature. He investigated both cases of constant pumping power and constant heat transfer rate for different operating conditions, nanoparticle diameters, and solid–liquid combinations. The fundamental result obtained is the existence of an optimal particle loading for either maximum heat transfer at constant driving power or minimum cost of operation at constant heat transfer rate. Roy et al. [16] investigated turbulent heat transfer and hydrodynamic behavior of various types of water-based nanofluids inside a typical radial flow cooling device numerically. They evaluated several turbulence models and choose the RANS-based k–ε SST turbulence model for subsequent simulations. Their results show that although heat transfer enhancement was found for all the types of nanofluids considered, their overall performance seems to indicate that their usage in practical applications may not be as beneficial as originally hoped for due to the corresponding increases in pumping power. Naik et al. [17] analyzed turbulent convection flow of CuO nanofluids of propylene glycol–water as the base fluid and flowing in a circular tube, subjected to a constant and uniform heat flux at the wall, numerically. They found that nanofluids containing more concentrations have shown higher heat transfer coefficient. They compared the numerical results with the experimental data and reasonable good agreement is achieved.

Lu et al. [18] investigated Large-eddy simulations (LES) of temperature fluctuations in a mixing tee with/without a porous medium. They find analysis of the temperature fluctuations and the power spectrum densities (PSD) at the locations having the strongest temperature fluctuations in the tee junction shows that the porous media significantly reduce the thermal fatigue effects. Bianco et al. [19] analyzed second law analysis of water nanofluid turbulent forced convection in a circular crosssection tube with constant wall temperature. Their results show that according to the inlet condition, there is a substantial variation of the entropy generation, particularly when Reynolds number is kept constant there is an increase of entropy generation, whereas when mass flow rate or velocity

is taken constant, entropy generation decreases. Leong et al. [20] investigated Entropy generation analysis of nanofluid flow in a circular tube subjected to constant wall temperature. Outcome of the analysis shows that titanium dioxide nanofluids offer lower total dimensionless entropy generation compared to that of alumina nanofluids. Recently, Bianco et al. [21] studied Entropy generation analysis of turbulent convection flow of Al_2O_3–water nanofluid in a circular tube subjected to constant wall heat flux. Their study shows that to minimize total entropy generation when velocity is kept constant, a low concentration of nanoparticles is necessary. Also Bianco et al. [22] analyzed numerical simulation of water/Al_2O_3 nanofluid turbulent convection. They find Heat transfer enhancement is increasing with the particle volume concentration and Reynolds number.

Framed in this general background, in the present paper, developing turbulent forced convection flow of Al_2O_3/water nanofluid in circular tube is numerically investigated. Steady state of a two-dimensional axial symmetric flow is considered and the channel is heated at uniform wall temperature. Investigation is conducted for different nanoparticle volume fraction, Reynolds number, and nanoparticle diameters. The finite volume method is employed to solve the problem and the two phase approach is used to evaluate the developing forced convection flow.

2. Nanofluid properties

Many studies have evaluated the nanofluids properties depending on both properties of base fluid and nanoparticles and according to them, several models have been proposed. Nanofluid density is obtained by measuring the volume and weight of the mixture. The particle volume fraction f can be estimated knowing the densities of both constituents [23]

$$\rho_{nf} = \varphi\rho_p + (1-\varphi)\rho_f \tag{1}$$

The specific heat of nanofluid can be determined by assuming thermal equilibrium between the nanoparticles and the base fluid as [23]:

$$(\rho c_p)_{nf} = (1-\varphi)(\rho c_p)_f + \varphi(\rho c_p)_p \tag{2}$$

Experimental data show that classical models such as those of Maxwell [24] and Hamilton–Crosser [25] for predicting thermal conductivity and Einstein [26,27], Brinkman [28], and Batchelor [29] for predicting the viscosity of nanofluids do not lead to accurate results [30]. These models include only the effect of the nanoparticle concentration and do not consider important mechanisms of heat transfer such as Brownian motion and do not employ temperature and size of nanoparticles. The heat transfer characteristics of nanomechanisms of fluids are dependent on effective viscosity and conductivity, etc.

Using regression analysis and based on different valid experimental data, Corcione [30] proposed the following empirical correlation for thermal conductivity with a standard deviation of less than 1.86%:

$$\frac{k_{nf}}{k_f} = 1 + 4.4\mathrm{Re}^{0.4}\mathrm{Pr}^{0.66}\left(\frac{T}{T_{fr}}\right)^{10}\left(\frac{k_p}{k_f}\right)^{0.03}\varphi^{0.66} \tag{3}$$

In Eq. (3), Pr and Re are

$$\mathrm{Pr} = \frac{\mu_f}{\rho_f \alpha_f}, \quad \mathrm{Re} = \frac{2\rho_f k_B T}{\pi \mu_f^2 d_p} \tag{4}$$

Corcione model for thermal conductivity has been proposed for nanofluids consisting of alumina, copper oxide, titanium and copper nanoparticles with diameter in the range between 10 and 150 nm suspended in water or ethylene glycol (EG) with volume fraction in the range from 0.002 to 0.09 and temperature in the range between 294 and 324 K.

Corcione model for viscosity is

$$\frac{\mu_{nf}}{\mu_f} = \frac{1}{1 - 34.87(d_p/d_f)^{-0.3}\varphi^{1.03}} \tag{5}$$

$$d_f = 0.1\left(\frac{6M}{Np\ \rho_{f0}}\right) \tag{6}$$

where d_f is the equivalent diameter of a base fluid molecule [30]. In which M is the molecular weight of the base fluid, N is the Avogadro number, and ρ_{f0} is the mass density of the base fluid calculated at temperature $T_0 = 293$ K.

Corcione model for viscosity was proposed for nanofluids consisting of alumina, titanium, silica oxides and copper nanoparticles with diameter ranging between 25 and 200 nm, suspended in water, ethylene glycol (EG), propylene glycol (PG) or ethanol (Eth) with nanoparticle volume fraction in the range from 0.0001 to 0.071 and temperature in the range between 293 and 333 K. When water is used as the base fluid its viscosity as a function of temperature is

$$\mu_f = 562.77(\ln(T + 62.756))^{-8.9137} \tag{7}$$

The thermo-physical properties of the base fluid and Al_2O_3 nanoparticles at 295 K are presented in Table 1 [31].

Corcione model [30] is used for evaluated conductivity and viscosity. In this model conductivity and viscosity are functions of temperature, and volume fraction and nanoparticle size are used for Al_2O_3–water nanofluid.

3. Governing equations

The schematic of geometry studied is shown in Fig. 1. The geometrical configurations consist of a tube with length (L) of 1 m and circular section with the diameter (D) equal to 0.02 (m). The problem under investigation is a two-dimensional, steady, forced turbulent convection flow of nanofluid flowing inside straight circular tubes. It is subjected to a constant and uniform temperature at the wall $T_w = 310$ K. At the tube inlet section, uniform axial velocity Vin, temperature $T_{in} = 300$ K turbulent intensity and hydraulic diameter have been specified. At the outlet section, the flow and temperature fields are assumed fully developed ($x/D > 10$). The Reynolds number was varied from 10,000 to 100,000.

The considered nanofluid is a mixture composed of water and particles of Al_2O_3, with a diameter of less than 100 nm. The nanofluid is treated, continuous and dilute Newtonian mixture which has variable physical properties. The compression work, dispersion and viscous dissipation are assumed negligible in the energy equation and heat conduction is represented by Fourier law. Furthermore, nanoparticles are in thermal equilibrium with the base fluid and there are not any external force, heat source, chemical reaction and radiative heat transfer in the problem.

Table 1 Thermophysical properties of the base fluid and the nanoparticles [31].

	β (K^{-1})	k ($W\,m^{-1}\,K^{-1}$)	c_p ($J\,kg^{-1}\,K^{-1}$)	ρ ($kg\,m^{-3}$)	d_p (nm)
Water	2.1×10^{-4}	0.613	4179	997.1	–
Al_2O_3	0.85×10^{-5}	40	765	3970	33

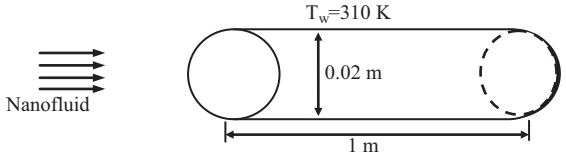

Figure 1 Schematic of the geometry studied.

For closure of the governing equations of fluid flow, empirical data or approximate models are required to express the turbulent stresses and heat flux quantities of the related physical phenomenon. In the present analysis, k–ε turbulent model was adopted. k–ε Turbulent model introduces two additional equations namely turbulent kinetic energy (k) and rate of dissipation (ε).

According to the aforementioned assumptions, governing equations including the continuity, the momentum, the energy and k-epsilon model equations are the followings.

The continuity equation is [32]

$$\frac{1}{r}\frac{\partial(rv_r)}{\partial r}+\frac{\partial(v_z)}{\partial z}=0 \tag{8}$$

The momentum equation [33] is

$$\frac{1}{r}v_r\frac{\partial(rv_r)}{\partial r}+v_z\frac{\partial v_r}{\partial z} =-\frac{1}{\rho}\frac{\partial p}{\partial r}+(\upsilon+\upsilon_t)\left[\frac{1}{r}\frac{\partial}{\partial r}\left(\frac{\partial(rv_r)}{\partial r}\right)+\frac{\partial}{\partial z}\left(\frac{\partial(v_z)}{\partial z}\right)\right] \tag{9}$$

$$v_z\frac{\partial(v_z)}{\partial z}+\frac{1}{r}v_r\frac{\partial(rv_z)}{\partial z} =-\frac{1}{\rho}\frac{\partial p}{\partial z}+(\upsilon+\upsilon_t)\left[\frac{1}{r}\frac{\partial}{\partial r}\left(\frac{\partial(rv_r)}{\partial r}\right)+\frac{\partial}{\partial z}\left(\frac{\partial(v_z)}{\partial z}\right)-\frac{v_r}{r^2}\right] \tag{10}$$

The energy equation [33] is

$$\frac{1}{r}\frac{\partial(v_rT)}{\partial r}+\frac{\partial(v_zT)}{\partial z}+=\frac{1}{r}\frac{\partial}{\partial r}\left(r\alpha_{eff}\frac{\partial T}{\partial r}\right)+\frac{\partial}{\partial z}\left(\alpha_{eff}\frac{\partial T}{\partial z}\right) \tag{11}$$

The k–ε turbulent equation [33] is

$$\frac{1}{r}v_r\frac{\partial(rk)}{\partial r}+v_z\frac{\partial k}{\partial z} =\left(\upsilon+\frac{\upsilon_t}{\sigma_k}\right)\left[\frac{1}{r}\frac{\partial}{\partial r}\left(\frac{\partial(rk)}{\partial r}\right)+\frac{\partial}{\partial z}\left(\frac{\partial k}{\partial z}\right)\right]+\frac{1}{\rho}G_k-\varepsilon \tag{12}$$

$$\frac{1}{r}v_r\frac{\partial(r\varepsilon)}{\partial r}+v_r\frac{\partial\varepsilon}{\partial z}=\left(\upsilon+\frac{\upsilon_t}{\sigma_\varepsilon}\right)\left[\frac{1}{r}\frac{\partial}{\partial r}\left(\frac{\partial(r\varepsilon)}{\partial r}\right)+\frac{\partial}{\partial z}\left(\frac{\partial\varepsilon}{\partial z}\right)\right] +C_{1\varepsilon}\frac{\varepsilon}{\rho k}G_k-C_{1\varepsilon}\frac{\varepsilon^2}{\rho k} \tag{13}$$

Table 2 Constants used in k–ε turbulence model.

C_μ	$C_{1\varepsilon}$	$C_{1\varepsilon}$	σ_k	σ_ε	σ_t
0.09	1.44	1.92	1.0	1.3	1.0

In these equations, G_k represents the generation of turbulence kinetic energy due to the mean velocity gradients, calculated as described in. $C_{1\varepsilon}$ and $C_{2\varepsilon}$ are constants. σ_k and σ_ε are the turbulent Prandtl numbers for k and ε, respectively and μ_t is the eddy viscosity and is modeled as

$$\mu_t=\rho C_\mu\frac{k^2}{\varepsilon} \tag{14}$$

The values for all constants appearing in the k and ε model are summarized in Table 2.

Local convective heat transfer coefficient on wall is

$$h=\frac{-k_{nf}\frac{\partial T}{\partial x}\big|_{wall}}{(T_w-T_b)} \tag{15}$$

The average Nusselt numbers, respectively, are

$$Nu_{ave}=\frac{hD}{k_f} \tag{16}$$

Reynolds number is defined as

$$Re=\frac{UD}{\nu_{f_0}} \tag{17}$$

4. Numerical procedure

The governing equations with the associated boundary conditions are numerically solved using the finite volume method [34]. The thermophysical properties such as thermal conductivity and viscosity, which are variable with temperature, are solved concurrently with flow, temperature in the whole solution domain. On the control volume faces these properties are averaged linearly using the calculated values on the grids. The SIMPLE algorithm has been adopted to solve for the pressure and the velocity components. The coupled sets of discretized equations have been solved iteratively using a line-by-line procedure.

Table 3 The average Nusselt number for different grids, φ = 0.01 and Re = 40,000.

Number of elements	Nu_{ave}	% Error
200×20	221.34	–
300×30	235.04	6.2
400×40	242.78	3.3
500×50	248.92	2.53
600×60	251.03	1

Axial symmetric flow is considered. In order to ensure the accuracy as well as the consistency of numerical results, several grids have been submitted to an extensive testing procedure for each of the cases considered.

Preliminary tests were carried out to test the accuracy of the numerical solution. To this scope four different grids were compared in terms of Nusselt number. The values of Nusselt number are reported in Table 3. It was found that independent result is obtained using 500×50. This grid density is therefore adopted for the present work and it is used for further analysis.

5. Validation

In order to validate the numerical procedure, the relations presented with Bejan [32], and the results are compared with the existing results in the literature.

Tables 4 and 5 show comparisons between the average Nusselt number and skin friction factor of the present work with the results of Bejan [32]. As it is observed from the tables, very good agreements exist between the results of present simulation and those of Bejan [32].

6. Results and discussion

Investigating the effect of nanoparticle volume fraction on the average Nusselt number, skin friction factor and pressure drop.

Here the effect of nanoparticle volume fraction on the average Nusselt number, skin friction factor and pressure drop is presented for $d_p = 33$ nm. Fig. 2 shows the variations of the average Nusselt number in terms of the Reynolds number for various volume fractions. For all the studied volume fractions, the average Nusselt number rises with increasing Reynolds number. This is acceptable because of increment of the conductivity of the nanofluid and subsequent improvement in heat transfer. The other reason of this increment in the average Nusselt number is acceleration of energy transport because of random motion of the nanoparticles (Brownian motion) inside the nanofluid. This process makes a more uniform temperature distribution inside the nanofluid and hence an improved heat transfer rate between the nanofluid and wall.

With increasing volume fraction up to 0.01 for a fixed Reynolds number, the average Nusselt number increases compared to pure water. The average Nusselt number values for the volume fraction of 0.02 have little difference with those of pure water. But during more increment of the volume fraction up to 0.04, the average Nusselt number decreases compared to pure water. This occurrence shows that for the studied turbulent regime inside tube and considering the applied conductivity model, the increment of the nanoparticle volume fraction from 0.02 to 0.04 has no increasing effect on the average Nusselt number. In fact in case of the turbulent regime, turbulence and the vortexes have more determinative role compared to the diffusion mechanism. Hence increment of the volume fraction of nanoparticles after 0.01 that causes improved conductivity and diffusivity, has no increasing effect on the average Nusselt number.

The most increment in the average Nusselt number for a fixed volume fraction takes place in volume fraction of 0.04, where the average Nusselt number rises up to sevenfold for an increment in Reynolds number from 10,000 to 100,000.

In Fig. 3 the skin friction factor variations are presented in terms of the Reynolds number for various volume fractions. The skin friction factor decreases with increasing Reynolds number for all the studied volume fractions. By increasing the Reynolds numbers the boundary layer thickness and consequently the frictional effects and thus c_f decrease. The skin friction factor increases with increasing nanoparticle volume fraction. This increment is more sensible for high Reynolds numbers. By increasing the nanoparticle volume fraction, viscosity of the nanofluid increases and consequently the skin friction rises. The least and most increment in the skin friction factor with increasing volume fraction for a fixed Reynolds number is equal to 3.9% and 5.01% and takes place at Reynolds numbers of 10,000 and 100,000 respectively.

Fig. 4 presents the pressure drop in terms of the Reynolds number for various volume fractions. The pressure drop decreases with the increment of Reynolds number. As can be seen in Fig. 4 the pressure drop of the nanofluid is greater than the pure fluid. The increment of nanoparticle volume fraction raises the pressure drop. The most and least pressure drop with increasing volume fraction for a fixed Reynolds number is equal to 15.59% and 16.87% and takes place at Reynolds numbers of 10,000 and 100,000 respectively. Increasing Reynolds number from 60,000 to 100,000 and with increasing volume fraction, the most pressure drop from 16.67% reaches to 16.87% compared to the pure fluid. It shows that with increment of the Reynolds number from 60,000 to 100,000, the increasing volume fraction has no noticeable effect on the pressure drop. In this range of the Reynolds number the pressure drop is more depended on the vortexes and secondary flows and the rising viscosity because of the increasing nanoparticle volume fraction has not a sensible effect on the pressure drop. If the increment in nanoparticle volume fraction in this range (0.01–0.04) causes the average Nusselt number to increase, the utilization of nanofluid with such volume fractions instead of pure fluid can be reasonable.

Table 4 Comparisons between the average Nusselt number results with the Bejan [32].

Re	Nu_{ave}, present work	$Nu_{ave} = 0.012\ (Re^{0.87}–280)Pr^{0.4}$ [32]	Percent difference %
20,000	132.45	129.83	2.02
40,000	246.8	243.04	1.55
60,000	352.8	348.77	1.15
80,000	453.32	449.93	0.75
100,000	550	547.82	0.4

Table 5 Comparisons between the skin friction factor results with the Bejan [32].

Re	c_f, present work	$c_f = 0.046\ (Re^{-0.2})$ [32]	Percent difference %
20,000	0.0063	0.0061	4.22
40,000	0.0055	0.0053	3.37
60,000	0.0051	0.0049	3.37
80,000	0.0048	0.0046	3.53
100,000	0.0046	0.0044	3.70

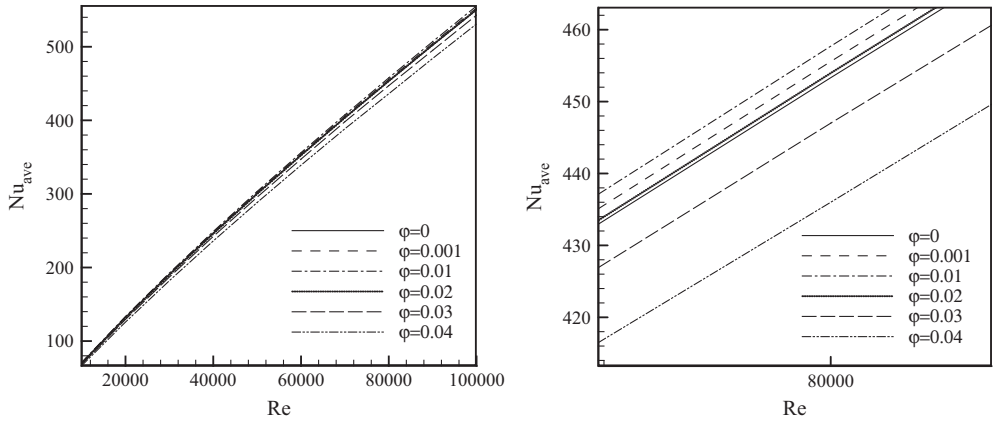

Figure 2 The variations of the average Nusselt number versus Reynolds number for various volume fractions (the diagram on the right is an enlarged view of the left side).

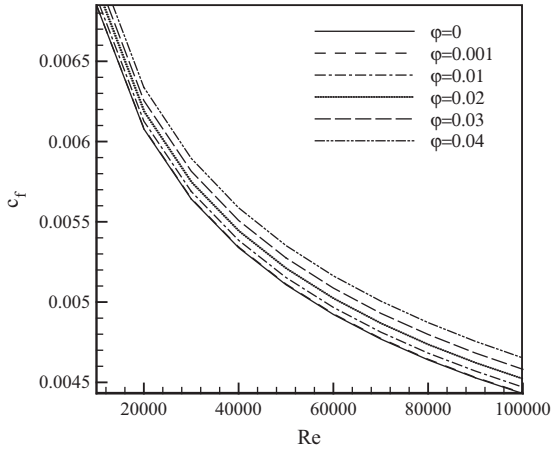

Figure 3 The variations of the skin friction factor versus Reynolds number for various volume fractions.

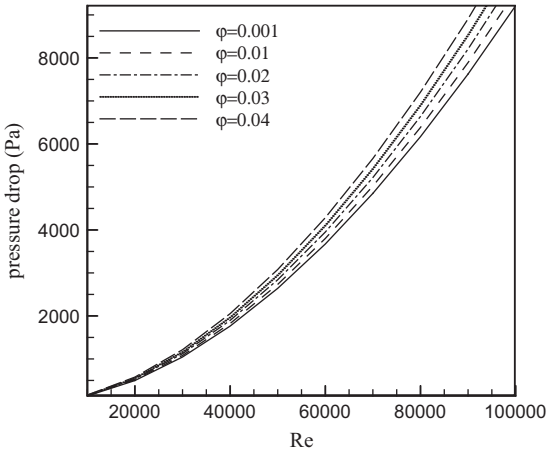

Figure 4 The variations of the pressure drop versus Reynolds number for various volume fractions.

6.1. Investigating the effect of nanoparticles' diameter on the average Nusselt number, skin friction factor and pressure drop

Fig. 5 shows the variations of the average Nusselt number in terms of Reynolds number in volume fraction of 0.01 for various values of nanoparticles' diameter (25–100 nm). With increasing nanoparticles' diameter the average Nusselt number has an insignificant decrease. The reason for this behavior should be searched in the random movement of nanoparticles (Brownian motion) inside the nanofluid. The more nanoparticles' movement inside the nanofluid increases, the more uniform temperature distribution inside nanofluid and hence, better heat transfer is achieved. With increasing nanoparticles' diameter, the Brownian motion weakens and the average Nusselt number decreases. Furthermore enlargement of the nanoparticles brings less surface to volume ratio between the nanoparticle and the fluid's molecules which itself reduce the heat exchange inside the nanofluid. The most and least reduction in the average Nusselt number with increasing nanoparticles' diameter is equal to 0.28 and 0.07 and takes place for the Reynolds numbers of 10,000 and 20,000 respectively.

Figs. 6 and 7 show the variations of the skin friction factor and pressure drop in terms of the Reynolds number for the volume fraction of 0.01 and for various nanoparticles' diameters.

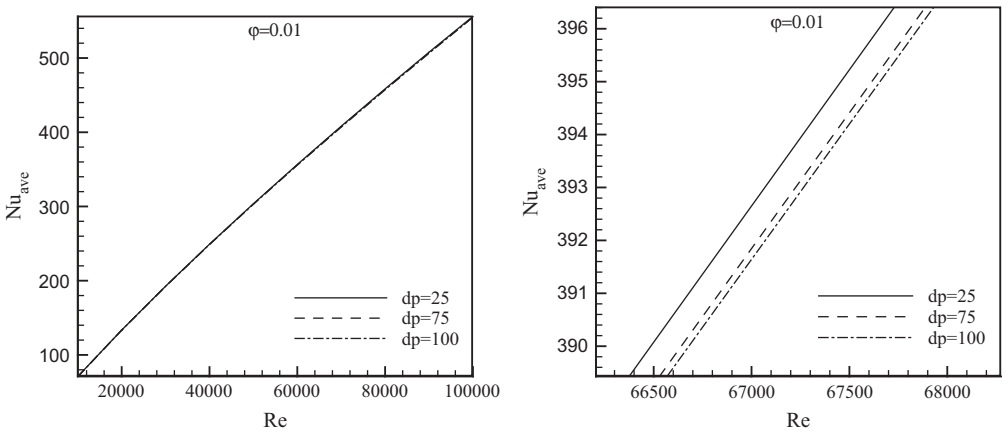

Figure 5 The variations of the average Nusselt number versus Reynolds number for various nanoparticles' diameter in $\varphi = 0.01$ (the diagram on the right is an enlarged view of the left side).

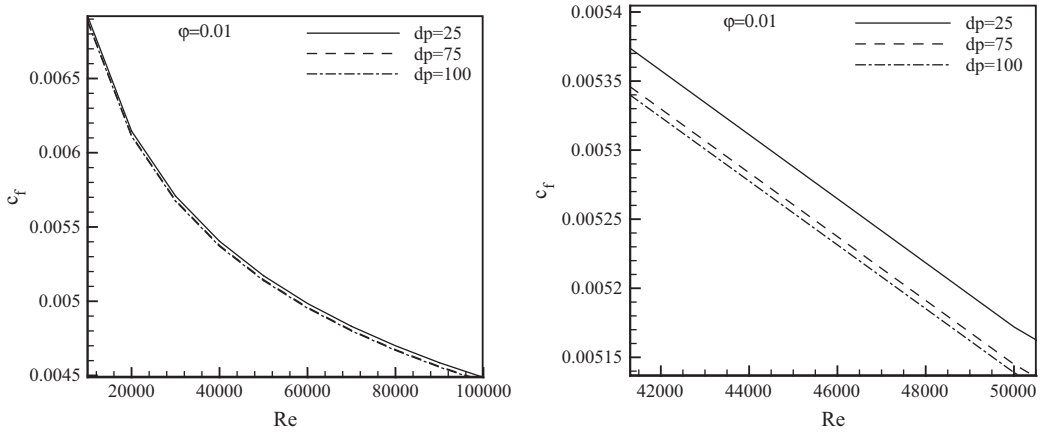

Figure 6 The variations of the skin friction factor versus Reynolds number for various nanoparticles' diameter in $\varphi = 0.01$ (the diagram on the right is an enlarged view of the left side).

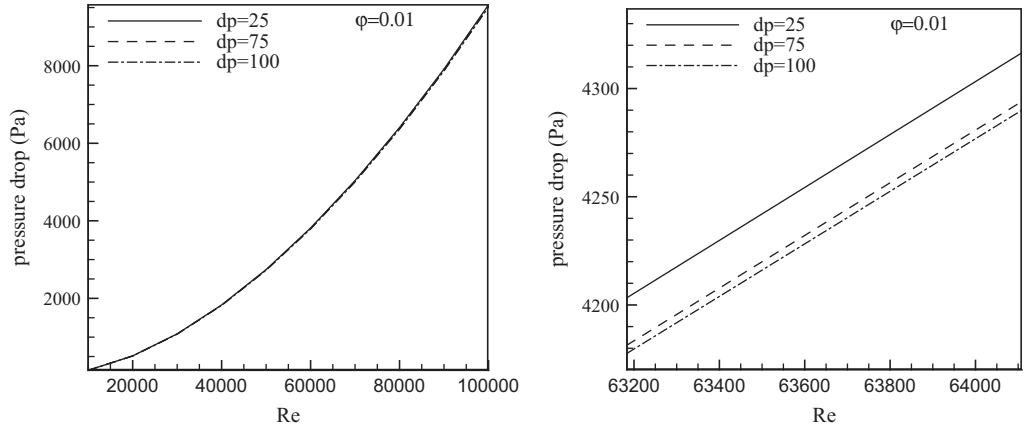

Figure 7 The variations of the pressure drop versus Reynolds number for various nanoparticles' diameter in $\varphi = 0.01$ (the diagram on the right is an enlarged view of the left side).

With increasing nanoparticles' diameter, the skin friction factor and pressure drop decrease. This behavior can be because of the reduction in the number of nanoparticles with increasing diameter. Reduction in the number of nanoparticles can reduce the chance of their impact on the walls and consequently reduces the friction effects. The most and least decrement of

the friction factor with increasing diameter of the nanoparticles is equal to 0.67% and 0.52% and takes place in Reynolds numbers of 10,000 and 100,000 respectively.

6.2. Introducing relations for average Nusselt number and skin friction factor in terms of Reynolds number and the nanoparticle volume fraction

In this part some relations are presented to compute average Nusselt number and skin friction factor in terms of Reynolds number and volume fraction of the nanoparticles by curve fitting on the present results. The relation of (18) gives the average Nusselt number variations in terms of the Reynolds number and nanoparticle volume fraction. The correlation factor (R^2) is equal to 0.998 which confirms the good agreement between this relation and present results.

$$\mathrm{Nu_{ave}} = (0.5277 \times 10^{-2})\mathrm{Re} + (0.1625 \times 10^{5})\varphi^2 + (0.3066 \times 10^{3})\varphi + 0.3084 \times 10^{2} \quad (18)$$

The relation of (19) gives the skin friction factor in terms of the Reynolds number and nanoparticle volume fraction. The correlation factor is equal to 0.996 which confirms the good agreement between this relation and present results.

$$c_f = (0.4296 \times 10^{-2}) \exp(1.361\varphi) + (0.3359 \times 10^{-2}) \times \exp(-0.2953 \times 10^{-4}\mathrm{Re}) \quad (19)$$

7. Conclusion

In this study the forced convection heat transfer of water–Al_2O_3 nanofluid inside a circular pipe for the Reynolds numbers of 10,000 to 100,000, nanoparticle volume fractions in a range of 0–0.04 and diameters of 25, 33, 75 and 100 nm has been considered. The lateral surface of the pipe is held at 310 °C and the inlet nanofluid flow is at 300 °C. Based on the numerical results,

(1) For all the studied volume fractions, the average Nusselt number increases with increasing Reynolds number.
(2) With increasing volume fraction up to 0.01 and for a fixed Reynolds number, the average Nusselt number compared to that of pure water increases, but afterward the average Nusselt number decreases with increasing volume fraction to 0.04.
(3) The most increment in the average Nusselt number for a fixed volume fraction takes place in volume fraction of 0.04, where the average Nusselt number rises up to sevenfold for an increment in Reynolds number from 10,000 to 100,000.
(4) The skin friction factor decreases with increasing Reynolds number for all the studied volume fractions. The most and least increment in the friction factor with increasing volume fraction for a fixed Reynolds number is equal to 3.9% and 5.01% and takes place at Reynolds numbers of 10,000 and 100,000 respectively.
(5) Increasing Reynolds number for all volume fractions causes the pressure drop to increase. The increment of nanoparticle volume fraction increases the pressure drop. The most and least pressure drop with increasing volume fraction for a fixed Reynolds number is equal to 15.59% and 16.87% and takes place at Reynolds numbers of 10,000 and 100,000 respectively.
(6) By the increment of the Reynolds number from 60,000 to 100,000, the increasing volume fraction has no noticeable effect on the pressure drop.
(7) With increasing nanoparticles' diameter the average Nusselt number has an insignificant decrease.
(8) With increasing nanoparticles' diameter, the skin friction factor and pressure drop decrease. The most and least decrement of the friction factor with increasing diameter of the nanoparticles is equal to 0.67% and 0.52% and takes place in Reynolds numbers of 10,000 and 100,000 respectively.
(9) The most and least pressure drop with increasing diameter of the nanoparticles is equal to 0.66% and 0.49% and takes place in Reynolds numbers of 20,000 and 80,000 respectively.

References

[1] Lee S, Choi S, Li S, Eastman JA. Measuring thermal conductivity of fluids containing oxide nanoparticles. ASME Trans J Heat Transfer 1999;121:280–9.
[2] Eastman JA, Choi S, Li W, Yu S, Thompson LJ. Anomalously increased effective thermal conductivities of ethylene glycol-based nanofluids containing copper nanoparticles. J Appl Phys Lett 2001;78:718–20.
[3] Xuan Y, Li Q. Heat transfer enhancement of nanofluids. Int. J. Heat Fluid Flow 2000;21:58–64.
[4] Pak B, Cho YI. Hydrodynamic and heat transfer study of dispersed fluids with submicron metallic oxide particle. Heat Transfer 1998;11:151–70.
[5] Buongiorno J. Convective transports in nanofluids. ASME Trans J Heat Transfer 2006;128:240–50.
[6] Williams W, Buongiorno J, Hu LW. Experimental investigation of turbulent convective heat transfer and pressure loss of alumina/water and zirconia/water nanoparticle colloids, nanofluids in horizontal tubes. J. Heat Transfer 2008;130:1–7.
[7] Namburu PK, Das DK, Tanguturi KM, Vajjha RS. Numerical study of turbulent flow and heat transfer characteristics of nanofluids considering variable properties. Int J Ther Sci 2009;48:290–302.
[8] Fotukian SM, Nasr Esfahany M. Experimental investigation of turbulent convective heat transfer of dilute c-Al_2O_3/water nanofluid inside a circular tube. Int. J. Heat Fluid Flow 2010;31:606–12.
[9] Fotukian SM, Nasr Esfahany M. Experimental study of turbulent convective heat transfer and pressure drop of dilute CuO/water nanofluid inside a circular tube. Int Commun Heat Mass Transfer 2010;37:214–9.
[10] Demir H, Dalkilic AS, Kurekci NA, Duangthongsuk W, Wongwises S. Numerical investigation on the single phase forced convection heat transfer characteristics of TiO_2 nanofluids in a double-tube counter flow heat exchanger. Int Commun Heat Mass Transfer 2011;38:218–28.
[11] Bianco V, Manca O, Nardini S. Numerical investigation on nanofluids turbulent convection heat transfer inside a circular tube. Int J Ther Sci 2011;50:341–9.
[12] Sajadi AR, Kazemi MH. Investigation of turbulent convective heat transfer and pressure drop of TiO_2/water nanofluid in circular tube. Int Commun Heat Mass Transfer 2011;38:1474–8.
[13] Zamzamian A, Nasseri S, Oskouie, Doosthoseini A, Joneidi A, Pazouki M. Experimental investigation of forced convective heat

transfer coefficient in nanofluids of Al_2O_3/EG and CuO/EG in a double pipe and plate heat exchangers under turbulent flow. Exp Ther Fluid Sci 2011;35:495–502.
[14] Nasiri M, Etemad SG, Bagheri R. Experimental investigation of turbulent flow and convective heat transfer characteristics of alumina water nanofluids in fully developed flow regime. Int Commun Heat Mass Transfer 2012;39:1272–8.
[15] Corcione M, Cianfrini M, Quintino A. Heat transfer of nanofluids in turbulent pipe flow. Int J Ther Sci 2012;56:58–69.
[16] Roy G, Gherasim I, Nadeau F, Poitras G, Nguyen CT. Heat transfer performance and hydrodynamic behavior of turbulent nanofluid radial flows. Int J Ther Sci 2012;58:120–9.
[17] Naik MT, Vojkani E, Ravi G. Numerical investigation of turbulent flow and heat transfer characteristics of PGW-CuO nanofluids. Int J Min Metall Mech Eng (IJMMME) 2013;2:141–5.
[18] Lua T, Jiangb PX, Guoa ZJ, Zhangb YW, Lib H. Large-eddy simulations (LES) of temperature fluctuations in a mixing tee with/without a porous medium. Int J Heat Mass Transfer 2010;53:4757–67.
[19] Bianco V, Mancab O, Nardini S. Second law analysis of Al_2O_3–water nanofluid turbulent forced convection in a circular cross section tube with constant wall temperature. Adv Mech Eng 2013:12. Article ID 920278.
[20] Leong KY, Saidura R, Mahliaa TMI, Yaua YH. Entropy generation analysis of nanofluid flow in a circular tube subjected to constant wall temperature. Int. Commun. Heat Mass Transfer 2012;39(8):1169–75.
[21] Biancoa V, Mancab O, Nardini S. Entropy generation analysis of turbulent convection flow of Al_2O_3–water nanofluid in a circular tube subjected to constant wall heat flux. Energy Convers Manage 2014;77:306–14.
[22] Biancoa V, Mancab O, Nardini S. Numerical simulation of water/Al_2O_3 nanofluid turbulent convection. Adv Mech Eng 2010:10. Article ID 976254.
[23] Chamkhaa AJ, Abu-Nada E. Mixed convection flow in single- and double-lid driven square cavities filled with water–Al_2O_3 nanofluid: effect of viscosity models. Euro J Mech B/Fluids 2012;36:82–96.
[24] Maxwell JC. A treatise on electricity and magnetism. 3rd ed. New York: Dover; 1954.
[25] Hamilton RL, Crosser OK. Thermal conductivity of heterogeneous two component systems. Ind Eng Chem Fundam 1962;1:187–91.
[26] Einstein A. Eine neue bestimmung der molekul-dimension (a new determination of the molecular dimensions). Ann. Phys. 1906;19:289–306.
[27] Einstein A, Berichtigung Z. Meiner arbeit: Eine neue bestimmung der molekul-dimension (correction of my work: a new determination of the molecular dimensions). Ann. Phys. 1911;34:581–92.
[28] Brinkman HC. The viscosity of concentrated suspensions and solutions. J Chem 1952;20:571–81.
[29] Batchelor G. The effect of Brownian motion on the bulk stress in a suspension of spherical particles. J Fluid Mech 1977;83:97–117.
[30] Corcione M. Empirical correlating equations for predicting the effective thermal conductivity and dynamic viscosity of nanofluids. Energy Convers. Manage. 2011;52:789–93.
[31] Alloui Z, Vasseur P, Reggio M. Natural convection of nanofluids in a shallow cavity heated from below. Int J Ther Sci 2010;50:1–9.
[32] Bijan A. Convection heat transfer. 3rd ed. New York: Wily; 1984.
[33] Roy G, Gherasim I, Nadeau F, Poitras G, Nguyen CT. Heat transfer performance and hydrodynamic behavior of turbulent nanofluid radial flows. Int J Ther Sci 2012;58:120–9.
[34] Patankar SV. Numerical heat transfer and fluid flow. In: Hemisphere. Washington (DC): McGraw-Hill; 1980.

Ghanbar Ali Sheikhzadeh is an Associate Professor of Mechanical Engineering Department at University of Kashan, Kashan, Iran. He received his PhD in Mechanical Engineering from Shahid Bahonar University of Kerman. His research work concerns numerical analysis and application of heat transfer in nano-systems and other areas of thermal and fluid sciences. Dr. Sheikhzadeh has published many journal and conference papers on these topics.

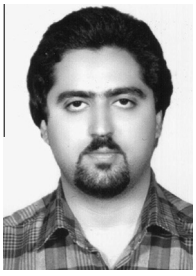

Alireza Aghaei is PhD Student of Mechanical Engineering at University of Kashan; Kashan, Iran. His research interest is computational fluid dynamics, heat transfer and solar energy.

Majid Dastmalchi is PhD Student of Mechanical Engineering at University of Kashan, Kashan, Iran. His research interest is computational fluid dynamics, heat transfer and combustion.

Hamed Forozande is MSC graduated of Mechanical Engineering at University of Kashan, Kashan, Iran. His research interest is heat transfer and combustion.